Stem Cell Reports

Article

Fibroblast growth factor 6 regulates sizing of the muscle stem cell pool

William Zofkie,[1] Sheryl M. Southard,[2] Thomas Braun,[3] and Christoph Lepper[1,*]

[1]Department of Physiology and Cell Biology, The Ohio State University, Columbus, OH, USA
[2]Seraxis Inc, Germantown, MD, USA
[3]Department of Cardiac Development and Remodeling, Max-Planck-Institute for Heart and Lung Research, Bad Nauheim, Germany
*Correspondence: christoph.lepper@osumc.edu
https://doi.org/10.1016/j.stemcr.2021.10.006

SUMMARY

Skeletal muscle stem cells, i.e., satellite cells (SCs), are the essential source of new myonuclei for skeletal muscle regeneration following injury or chronic degenerative myopathies. Both SC number and regenerative capacity diminish during aging. However, molecular regulators that govern sizing of the initial SC pool are unknown. We demonstrate that fibroblast growth factor 6 (FGF6) is critical for SC pool scaling. Mice lacking FGF6 have reduced SCs of early postnatal origin and impaired regeneration. By contrast, increasing FGF6 during the early postnatal period is sufficient for SC expansion. Together, these data support that FGF6 is necessary and sufficient to modulate SC numbers during a critical postnatal period to establish the quiescent adult muscle stem cell pool. Our work highlights postnatal development as a time window receptive for scaling a somatic stem cell population via growth factor signaling, which might be relevant for designing new biomedical strategies to enhance tissue regeneration.

INTRODUCTION

Skeletal muscle tissue possesses a tremendous capacity to repeatedly regenerate after acute injuries (Luz et al., 2002). The source of this regenerative capacity are the satellite cells (SCs), initially discovered and named after their localization, beneath the basal lamina on muscle fibers (Mauro, 1961). Several different lines of evidence cement their status as *bona fide* skeletal-muscle-resident stem cells. Labeling and tracing of proliferative cells with [3H] thymidine during muscle development and regeneration demonstrated that new nuclei occur first in the SC compartment followed by myonuclei (Moss and Leblond, 1970; Reznik, 1969; Snow, 1977). Identification of the transcription factor PAX7 as a specific biomarker of SCs prompted regeneration studies in *Pax7* germline mutant mice, which have severely compromised SC numbers and fail to regenerate muscle after acute injury (Oustanina et al., 2004; Seale et al., 2000). Transplantation of single myofibers with their associated cohort of SCs, and eventually single isolated SCs, into irradiated muscle demonstrated their ability to act as a source of regeneration (Collins et al., 2005; Sacco et al., 2008). Finally, PAX7^{+} cell lineage-tracing and cell ablation studies provided the ultimate *in vivo* proof that they are the essential source of new myonuclei for regenerative myogenesis (Lepper et al., 2009, 2011; McCarthy et al., 2011; Murphy et al., 2011; Sambasivan et al., 2011).

SCs have an embryonic origin; they derive from a somatic population of PAX3^{+}/PAX7^{+} myogenic progenitor cells (Gros et al., 2005; Lepper and Fan, 2010; Relaix et al., 2005, 2006; Schienda et al., 2006). During secondary myogenesis, PAX3^{+}/PAX7^{+} progenitors undergo an epithelial to mesenchymal transition and delaminate from the central domain of the dermomyotome "parachuting"

down into the underlying myotome (Gros et al., 2005; Relaix et al., 2005). They maintain a highly proliferative state throughout development and into early postnatal development providing a source of cells that differentiates and fuses with primary and secondary myofibers to promote their growth (Relaix et al., 2005, 2006). Late in embryonic development (~mouse embryonic day 16.5), a basal lamina forms that encapsulates individual muscle fibers and associated myogenic progenitor cells, an event that establishes the SC niche (and by extension the SCs) (Ontell and Kozeka, 1984; Rosen et al., 1992). At birth, ~30% of all sub-laminal nuclei are SCs in murine skeletal muscle (Allbrook et al., 1971; Hellmuth and Allbrook, 1971; Schultz, 1974). During the early postnatal period, SCs are highly proliferative and drive muscle growth via differentiation and fusion with muscle fibers (Lepper et al., 2009; White et al., 2010). As SCs divide, differentiate, and fuse with the myofiber, the relative proportions change, and, in adult muscle, the percentage of SC nuclei drops to ~3% (Ontell et al., 1984), which are maintained in a mitotically quiescent state (Grounds and McGeachie, 1989; Schultz et al., 1978). It is the small population of SCs that escapes myogenic differentiation and instead transitions into a mitotically quiescent state that acts as a reserve of relatively undifferentiated muscle stem cells for regenerative myogenesis in the adult. SCs are found at similar densities in individual muscles (Boldrin and Morgan, 2012), which suggests that the process of reserving SCs is not random but tightly regulated. However, the molecular regulation of this scaling of the adult muscle stem cell pool, which is critical for the regenerative capacity of skeletal muscles, is not known and is the focus of this study.

Fibroblast growth factors (FGFs) comprise a large family of cell signaling proteins that regulate a wide variety of

processes, including cell proliferation, migration, and differentiation in both embryonic development and adult homeostatic contexts (Ornitz and Itoh, 2001). The large majority of FGFs can be secreted and signal in autocrine or paracrine fashion via binding and activation of their cognate cell surface receptors; i.e., FGF receptors (FGFRs) 1–4. SCs express high levels of FGFR1 and FGFR4, and several FGF ligands stimulate SC proliferation *in vitro* (Cornelison et al., 2001; Kastner et al., 2000; Sheehan and Allen, 1999; Yablonka-Reuveni et al., 2015). Conversely, overexpression of a dominant negative FGFR1 in the chick embryo resulted in severe disruptions of muscle development (Flanagan-Steet et al., 2000). While these data suggest that FGFR signaling is critical in myogenesis, the precise contribution of specific FGFs and FGFRs to the regulation of SCs and myogenesis *in vivo* remains unclear to date. For example, genetic ablation of FGFR1 in the skeletal muscle lineage had surprisingly little effect on SC numbers and regenerative capacity (Yablonka-Reuveni et al., 2015), possibly due to redundancy with FGFR4, which requires future investigation. Similarly, several FGFs are expressed in the skeletal muscle lineage, including FGF1, FGF2, FGF4, FGF5, FGF6, and FGF7 (Hannon et al., 1996; Kastner et al., 2000), but gene inactivation of individual FGFs in the mouse has mostly resulted in little or no disruption of muscle development (Pawlikowski et al., 2017). FGF6 is of particular interest due to its skeletal muscle lineage-specific expression pattern both in development and regeneration (Han and Martin, 1993; Zhao and Hoffman, 2004). However, conflicting reports on the regenerative capacity of *Fgf6* mutant mice more than two decades ago had left the role of FGF6 in regeneration unresolved (Fiore et al., 2000; Floss et al., 1997). We reason that the earlier studies did not take into account the possible timing of FGF6 action during the postnatal period, which we have shown to be a receptive time window for increasing the size of the SC pool (Southard et al., 2016), which eventually affects regeneration in the adult.

Here we report that FGF6 is necessary for scaling of the SC pool and sufficient to modulate SC numbers during early postnatal development *in vivo*. We use a genetic approach to investigate the contributions from *Fgf6* to the regulation of both muscle fiber and SC pool sizes. Our data demonstrate a robust reduction in SCs across all analyzed muscle groups without affecting developmental growth of muscle fibers and reduced regenerative capacity in *Fgf6* mutant mice. Finally, we use exogenous delivery of FGF6 protein to growing skeletal muscle and discover increased SC numbers in the injected muscles. Our work not only clarifies the role of FGF6 from previous published studies for the field but also highlights plasticity during early postnatal development, which facilitates fine-tuning of the sizing of a somatic stem cell population via paracrine growth factor signaling.

RESULTS

SC hypoplasia in *Fgf6* mutant mice

To determine if FGF6 contributes to the regulation of SC pool size, we investigated whether the number of SCs is altered in *Fgf6* mutant mice. We chose three hindlimb muscles for analysis based on differential fiber type composition; i.e., the soleus (predominantly slow-twitch oxidative fibers), the extensor digitorum longus (EDL; predominantly fast-twitch glycolytic fibers), and the tibialis anterior (TA; mixed fast- and slow-type fibers). We also included the diaphragm in this analysis for its continuous rhythmic contractions. For SC detection, we performed dual anti-PAX7 (*bona fide* SC marker) and anti-Laminin (SC niche) immunofluorescence (IF) on cryopreserved cross sections from diaphragm, EDL, soleus, and TA muscles of 3-month-old wild-type (Wt) and *Fgf6*$^{-/-}$ sibling mice (Figures 1A–1H). Quantification of sub-laminal PAX7$^+$ cells revealed a significant reduction in SCs in *Fgf6*$^{-/-}$ muscles (Figure 1I). In male mice, all four skeletal muscle groups displayed a similar magnitude of SC reduction, ranging from ~31% in the soleus to ~49% reduction in the TA (Figure 1J). The SC reduction in *Fgf6* mutant mice is evident across both genders. Quantification of SCs in TA muscles from female Wt and *Fgf6*$^{-/-}$ sibling mice revealed a similar fold difference of ~36% (Figure 1J). The substantial reduction of SCs across multiple skeletal muscle groups in *Fgf6* mutant mice reveals a role for *Fgf6* in the regulation of SC pool size, which was not noticed in the initial report on SC numbers in *Fgf6* mutant mice, since no reliable SC marker, such as PAX7, was available at that time, and SC quantifications depended on transmission electron microscopy, preventing quantitative analysis of larger SC numbers (Floss et al., 1997).

No histological anomalies or myofiber size differences in *Fgf6* mutant mice under baseline conditions

To investigate whether FGF6 contributes to myofiber development and maintenance, we compared skeletal muscle tissue of 3-month-old Wt and *Fgf6*$^{-/-}$ littermates via histological staining of cryosections with hematoxylin and eosin (H&E). We did not detect any evidence for histopathological features in *Fgf6*$^{-/-}$ muscles. Myonuclei showed regular peripheral localization to the sarcolemma, and no excess fibrosis or inflammation was evident in the interstitial space similar to Wt controls (Figures 2A–2H'). Next, we compared myofiber sizes between Wt and *Fgf6*$^{-/-}$ littermates. For this, we performed anti-Laminin IF on cryopreserved cross sections of all four muscle groups and conducted semi-automated measurements of myofiber cross-sectional areas via SMASH, semi-automatic muscle analysis using segmentation of histology (Smith and Barton, 2014). We did not find any significant differences in
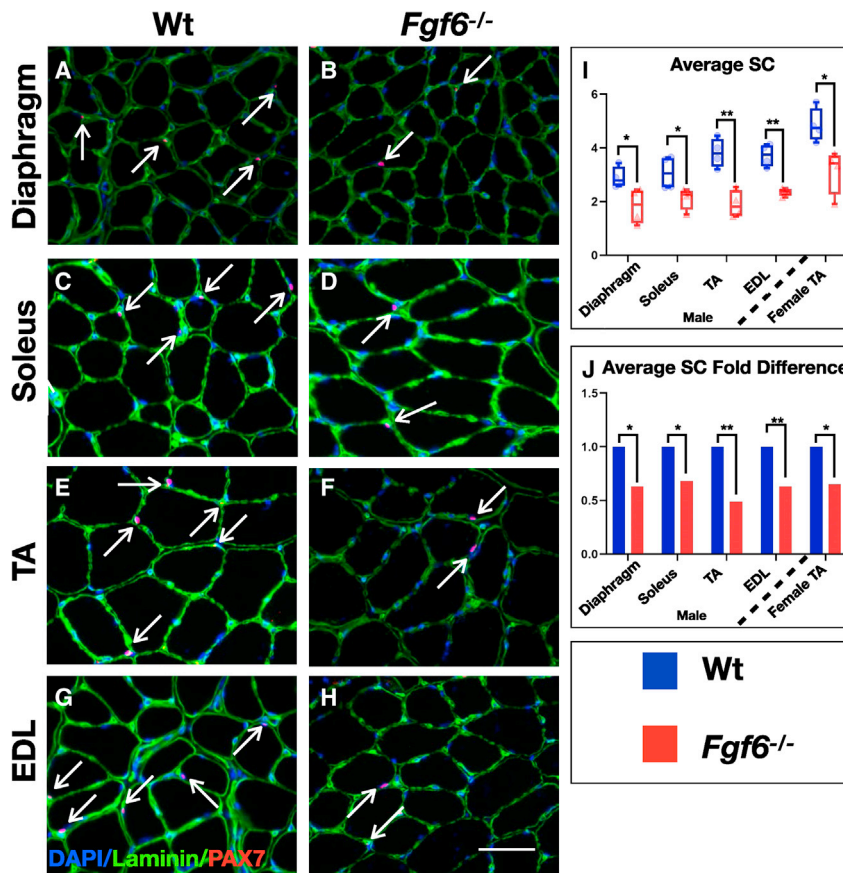
Figure 1. SC hypoplasia in *Fgf6* mutant mice

(A–H) Representative dual anti-PAX7/anti-Laminin IF stainings on 10-μm cryosections from diaphragm (A and B) and hindlimb muscle groups: soleus (C and D), TA (E and F), and EDL (G and H) from 3-month-old male Wt (A, C, E, and G) and *Fgf6*$^{-/-}$ mice (B, D, F, and H) at 40× magnification; arrows indicate PAX7 (red)-positive nuclei (blue) within the basal lamina (green); scale bar in (H), 50 μm. (I and J) Quantification of average SC numbers per 0.155-mm^2 area of 10-μm cryosections (I) and normalized as fold difference (J) from male Wt and *Fgf6*$^{-/-}$ diaphragm, soleus, TA, and EDL muscles, and female Wt and *Fgf6*$^{-/-}$ TA muscles (n = 4 adult mice for each genotype); paired two-tailed Student's t test: *p < 0.05; **p < 0.01.

average myofiber area (Figure 2I) or minimal Feret diameter (Figure 2J). For the EDL, myofibers extend the entire length of the muscle, hence allowing accurate quantification of total myofiber number in cross sections. We did not detect any significant differences in total EDL myofiber number in *Fgf6* mutant compared with Wt siblings (Figure 2K). Quantification of myonuclei in diaphragm, soleus, TA, and EDL muscles—via counts of DAPI-stained nuclei within myofibers identified by anti-dystrophin IF stainings—did not reveal any significant differences between *Fgf6* mutant and Wt control mice, suggesting that the myonuclear domain is not altered in *Fgf6* mutant mice (Figure 2L). Altogether, we conclude that *Fgf6* does not have an essential role in regulating embryonic muscle fiber development or postnatal muscle growth. The muscle fiber size quantifications across four skeletal muscle groups extend a previous qualitative assessment that H&E-stained muscle sections were indistinguishable between *Fgf6* mutant and Wt mice (Floss et al., 1997).

SCs become reduced in *Fgf6* mutant mice during early postnatal development

SCs gradually cease to proliferate and differentiate as myofibers complete acquisition of the adult myonuclear content during early postnatal mouse development between 2 and 3 weeks after birth via SC fusion (Lepper et al., 2009; White et al., 2010). Hence, this period appears to be critical for reserving SCs for skeletal muscle repair and regeneration in adulthood. Our prior work demonstrated that this period is receptive for increasing the size of the SC pool (Southard et al., 2016). To determine whether reduction of SCs is a product of early postnatal SC pool mis-scaling, we examined this period in *Fgf6*$^{-/-}$ mice. SCs were quantified in hindlimb muscles of Wt and *Fgf6*$^{-/-}$ sibling mice at 1 and 2 weeks after birth following the protocol used for 3-month-old mice. At 1 week after birth, we did not find any differences in the numbers of sub-laminal PAX7$^+$ SCs in *Fgf6*$^{-/-}$ compared with Wt control siblings (Figures 3A–3B‴, 3E, and 3F). By contrast, a significant SC reduction was evident in hindlimb muscles from 2-week-old *Fgf6*$^{-/-}$ mice (Figures 3C, 3D‴, 3G, and 3H). The magnitude of this reduction at ~40% was similar to the fold difference in SCs of 3-month-old *Fgf6*$^{-/-}$ mice (Figures 3H and 1J). These data demonstrate that the pool of SCs is mis-scaled during the second week after birth in *Fgf6*$^{-/-}$ mice.

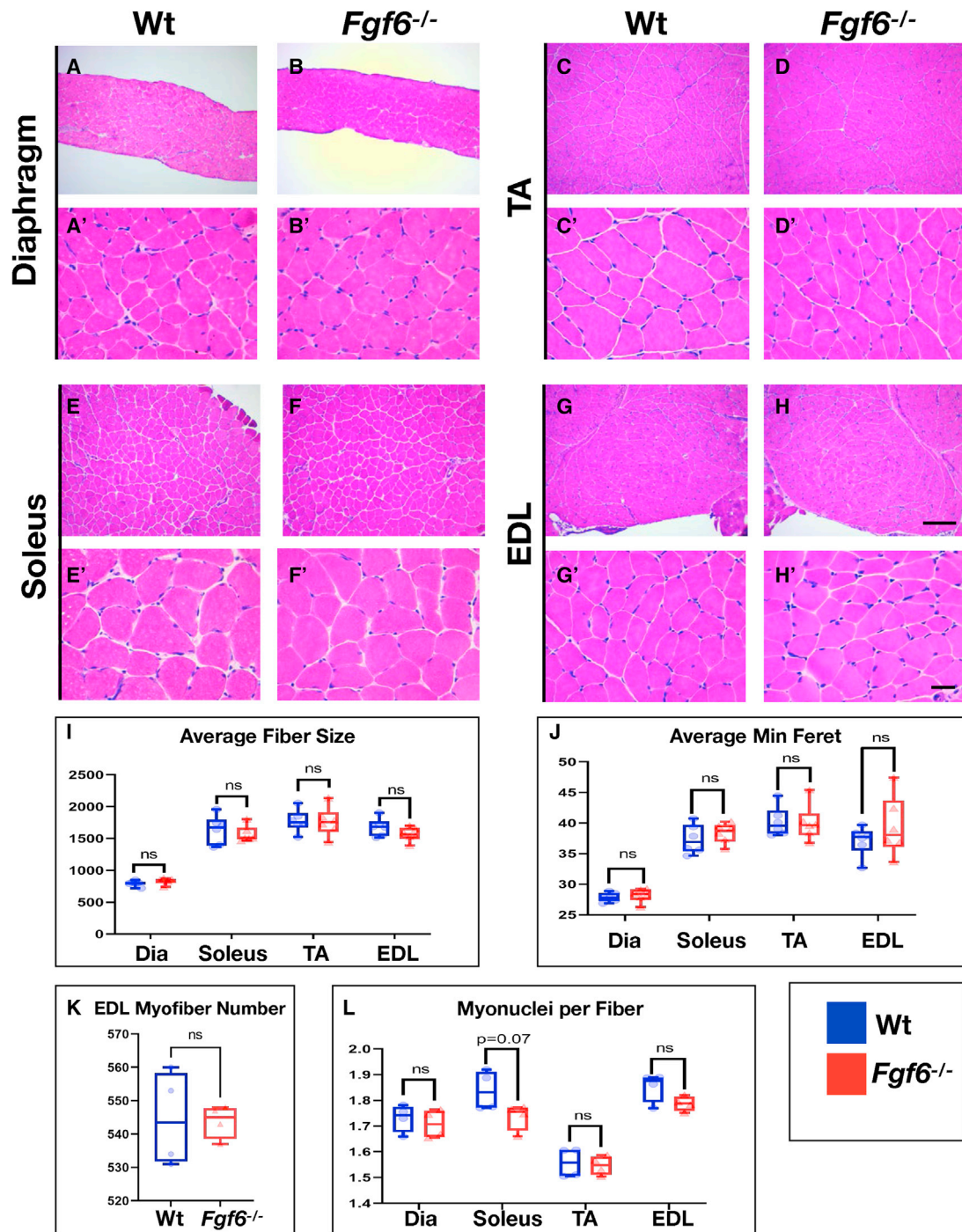FGF6 stimulates primary myoblast proliferation *in vitro* (Kastner et al., 2000). To determine whether SC

Figure 2. No histological anomalies or myofiber size differences in *Fgf6* mutant mice under baseline conditions

(A–H′) Representative images of H&E-stained 10-μm cryosections from diaphragm (A and B′), TA (C and D′), soleus (E and F′), and EDL (G and H′) from adult (3-month-old) male Wt (A, C, E, and G) and *Fgf6*$^{-/-}$ mice (B, D, F, and H) at 10× magnification (A–H) and 40× magnification (A′–H′); scale bar for 10× images in (H), 100 μm, and for 40× images in (H′), 10 μm.

(I) Average muscle fiber sizes in μm^2 for diaphragm (Dia), soleus, TA, and EDL muscles; n = 6 adult mice for each genotype.

(J) Average minimum Feret diameter in μm for diaphragm (Dia), soleus, TA, and EDL muscles; n = 6 adult mice for each genotype.

(K) Total EDL muscle fiber number; n = 4 3-month-old mice for each genotype; paired two-tailed Student's t test: not significant (ns), p > 0.05.

(L) Myonuclei count normalized to muscle fibers for diaphragm (Dia), soleus, TA, and EDL muscles; n = 4 3-month-old mice for each genotype; paired two-tailed Student's t test: not significant (ns), p > 0.05.
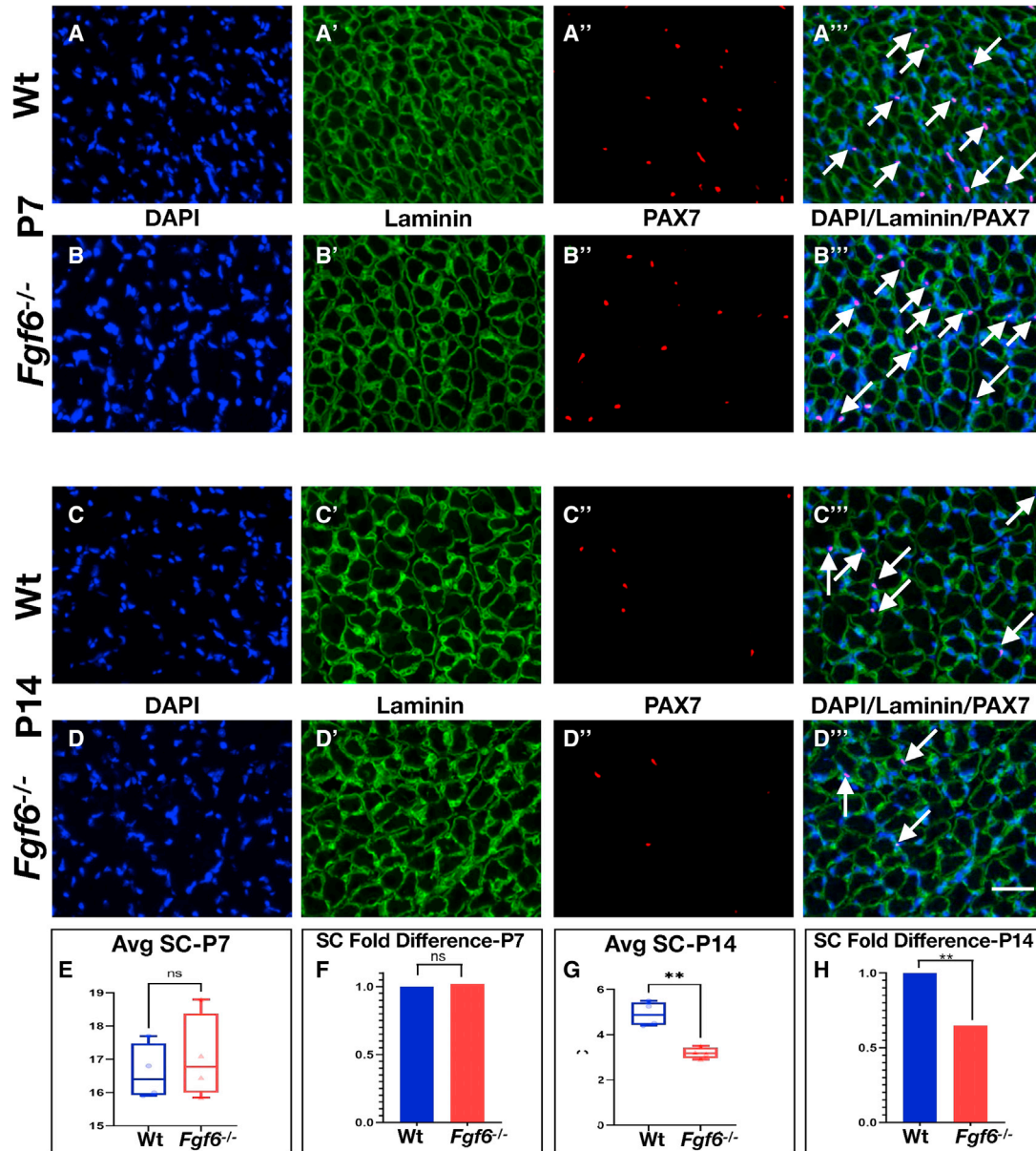
Figure 3. SC hypoplasia emerges during perinatal stages in *Fgf6* mutant mice

(A–D‴) Representative dual anti-PAX7/anti-Laminin IF stainings on 10-μm cryosections from Wt (A–A‴, C–C‴) and *Fgf6*$^{-/-}$ (B–B‴, D–D‴) lower hindlimb muscles at postnatal day 7 (P7, A and B‴) and day 14 (P14, C and D‴). Individual images for DAPI (blue, (A–D), Laminin (green, A′–D′), Pax7 (A″–D″), and the merged overlay (A‴–D‴) are shown at 20× magnification; scale bar in (D‴), 50 μm.

(E–H) Average SC numbers per 0.155-mm² area of 10-μm hindlimb muscle cryosections (E and G) and normalized as fold difference (F and H) from P7 (E and F) and P14 (G and H); n = 4 adult male mice for each genotype; paired two-tailed Student's t test: not significant (ns), p > 0.05; **p < 0.01.

proliferation is altered in *Fgf6*$^{-/-}$ mice, we conducted short-term *in vivo* proliferation assays via the thymidine analogue 5-ethynyl-2′-deoxyuridine (EdU). At 1 week after birth, we did not detect any significant differences in the percentage of EdU⁺/PAX7⁺ cells in hindlimb muscles from *Fgf6*$^{-/-}$ compared with Wt sibling mice (Figures 4A, 4B″, and 4E).

By contrast, at 2 weeks after birth, we found SC proliferation to be significantly reduced in hindlimb muscle of *Fgf6*$^{-/-}$ compared with Wt sibling mice (Figures 4C, 4D″, and 4F). The timing of reduced proliferation coincides with the initial reduction in SCs in *Fgf6*$^{-/-}$ mice, suggesting that compromised SC proliferation during an early
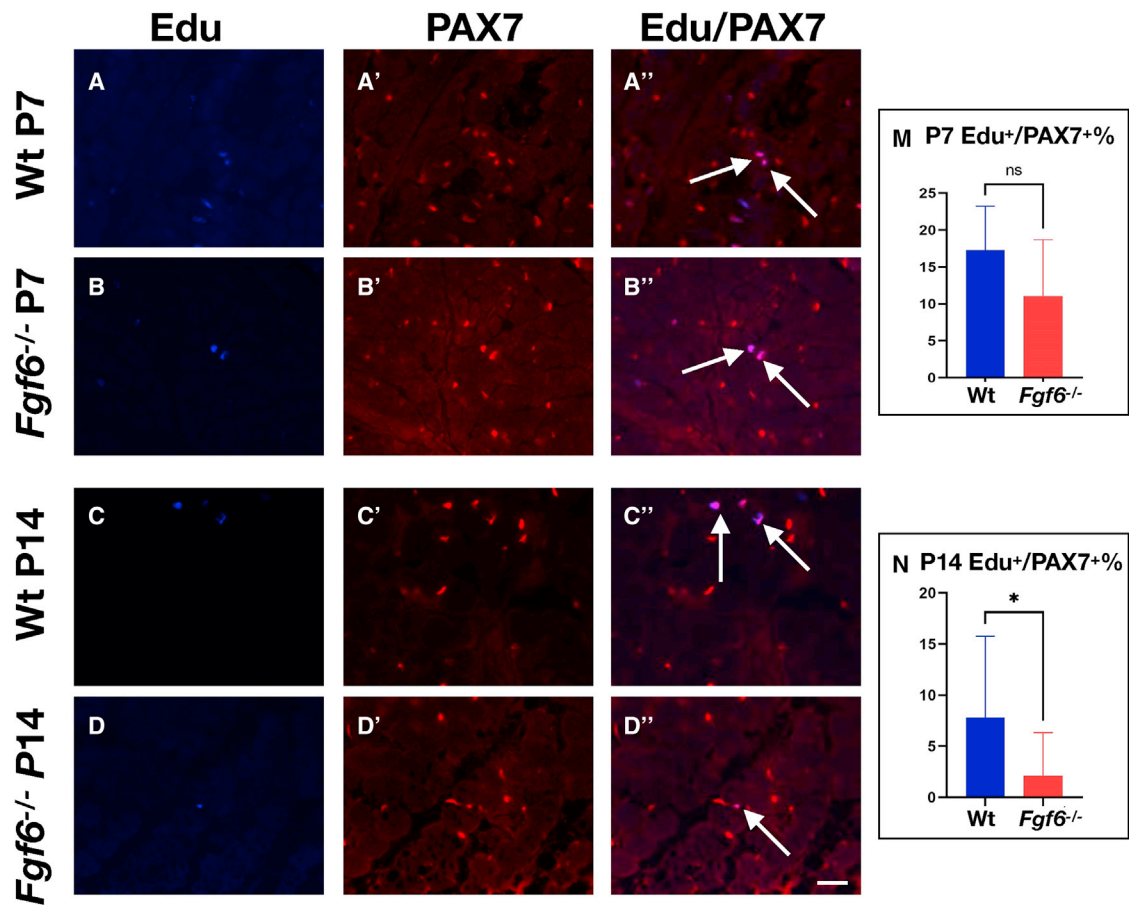
Figure 4. Reduced SC proliferation in *Fgf6* mutant mice at P14

(A–D″) Representative images of anti-PAX7 IF and EdU stainings on 10-μm cryosections from Wt (A–A″, C–C″) and *Fgf6*$^{-/-}$ (B–B″, D–D″) lower hindlimb muscles at postnatal day 7 (P7, A–B″) and day 14 (P14, C–D″). Individual images for EdU (blue, (A–D), PAX7 (red, A′–D′), and the merged overlay (A″, B″, C″, D″) are shown at 20× magnification; arrows indicate nuclei labeled with both EdU and PAX7; scale bar in (D″), 50 μm.

(E and F) Quantification of PAX7$^+$ SCs positive for EdU per 0.155-mm^2 area of 10-μm cryosections at P7 (E) and P14 (F) from Wt and *Fgf6*$^{-/-}$ hindlimb muscles; n = 4 early postnatal mice for each genotype; paired two-tailed Student's t test: *p < 0.05.

postnatal developmental window results in the reduced SC pool size in adulthood.

Injury-induced muscle regeneration is compromised in *Fgf6* mutant mice

The substantial reduction of SCs in *Fgf6* mutant mice prompted us to probe for the regenerative capacity of *Fgf6*$^{-/-}$ muscle. For this, the right TA muscles of 3-month-old Wt and *Fgf6*$^{-/-}$ sibling mice were injured via intra-muscular delivery of cardiotoxin (see experimental procedures). To measure the early regenerative response, we analyzed regenerating TA muscles at 3.5 and 5 days post injury (DPI). Histological analysis via H&E staining revealed similar kinetics of initial regenerative myotube formation between *Fgf6*$^{-/-}$ and Wt sibling mice. Small, centrally nucleated myotubes were evident as early

as 3.5 DPI in both groups (Figures 5A and 5D). At 5 DPI, the regeneration of TA muscles had progressed at a similar pace in *Fgf6*$^{-/-}$ compared with Wt mice. Regenerated muscles in both *Fgf6*$^{-/-}$ and Wt mice featured substantially larger myotubes compared with the earlier regeneration time point, but still contained an expanded interstitial content compared with uninjured muscle tissue (Figures 5B and 5E). Applying a similar approach as we have used for quantification of myofiber size of uninjured muscle fibers (see above, Figure 2), we determined average size and minimal Feret diameter of regenerated myotubes at both 3.5 and 5 DPI (Figures 5G, 5H, 5J, and 5K). No significant differences were detected between *Fgf6*$^{-/-}$ and Wt mice, suggesting that early steps in regenerative myogenesis are not affected in *Fgf6* mutant mice. For regeneration endpoint studies, we harvested regenerated TA muscles at 21 DPI.
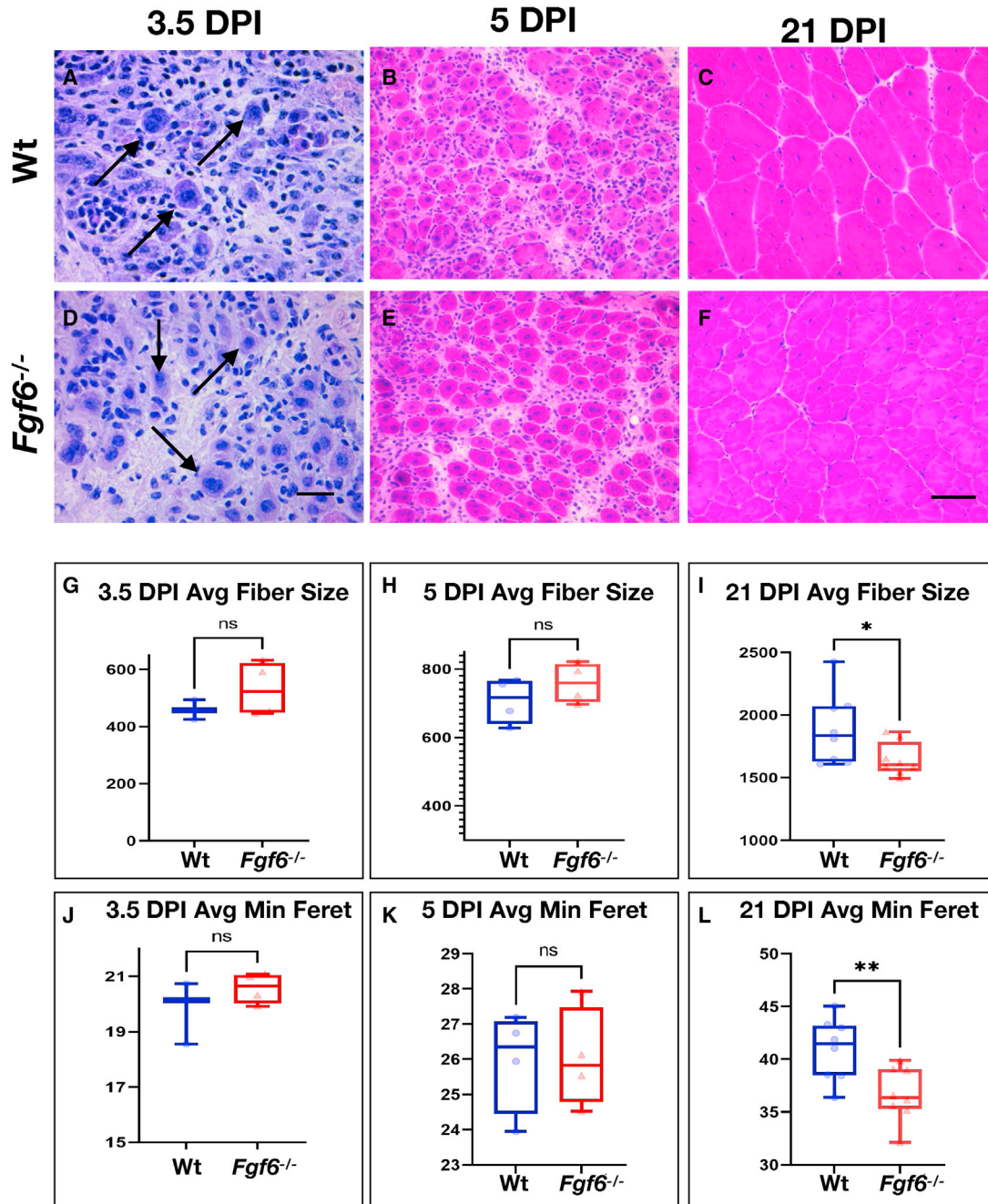
Figure 5. Injury-induced muscle regeneration is compromised in *Fgf6* mutant muscles

(A–F) Representative images of H&E-stained 10-µm cryosections from Wt (A–C) and *Fgf6*$^{-/-}$ (D–F) TA muscles at 3.5 DPI (A, D), 5 DPI (B, E), and 21 DPI (C, F) post injury via intra-muscular cardiotoxin delivery; scale bar for (A, D) in (D), 20 µm; scale bar for (B, C, E, and F) in (F), 50 µm.

(G–L) Quantification of regenerative TA myofiber sizes in µm^2 (G–I) and minimum Feret in µm (J–L) of Wt and *Fgf6*$^{-/-}$ mice at 3.5 DPI (G and J), 5 DPI (H and K), and 21 DPI (I–L); n = 3–8 adult male mice per genotype and regeneration time point; paired two-tailed Student's t test: not significant (ns), p > 0.05; *p < 0.05; **p < 0.01.

Histological analysis revealed skeletal muscle architecture similar to uninjured tissue in both *Fgf6*$^{-/-}$ and Wt mice, with the obvious exception of central nucleation of regen- erated myofibers (Figures 5C and 5F). However, we noted that regenerated myofibers appeared smaller in size in *Fgf6*$^{-/-}$ compared with Wt mice. To confirm this, we

quantified both average myofiber size and minimal Feret diameter and found a significant reduction in regenerated $Fgf6^{-/-}$ myofiber size compared with the control (Figures 5I and 5L). These data reveal that $Fgf6$ is necessary for full reconstitution of regenerative myofiber size after acute injury.

SC hypoplasia persists after injury-induced muscle regeneration

We next sought to determine whether FGF6 is required for maintaining the SC pool through the acute-injury-induced regeneration cycle. Thus, we performed dual anti-PAX7 and anti-Laminin IF on cryosections from 21 DPI $Fgf6^{-/-}$ and Wt regenerated TA muscles. Sub-laminal PAX7$^+$ SCs were present in skeletal muscle regenerates of both $Fgf6^{-/-}$ and Wt mice (Figures 6A and 6B). Quantification of sub-laminal PAX7$^+$ cells revealed that the SC pool remains reduced after injury-induced regeneration in $Fgf6^{-/-}$ mice, showing a magnitude in SC reduction similar to uninjured $Fgf6^{-/-}$ skeletal muscle (Figures 6C and 6D). These data indicate that the reduced SC pool size is stably maintained in $Fgf6$ mutant mice through an injury-induced regeneration bout. To determine whether these SCs retain stem cell self-renewal capacity, we analyzed their ability to repeatedly regenerate myofibers over three consecutive injuries to the same TA muscle, each 3 weeks apart. Histological analysis of triply regenerated skeletal muscle revealed the presence of regenerative myofibers (via central nucleation) and tissue architecture that was highly similar between $Fgf6^{-/-}$ and Wt muscles (Figures 6E and 6F). We did not find any signs of regeneration failure such as excess fibrosis or immune cell infiltration in any of the muscle regenerates. Quantification of average size and minimal Feret diameter of regenerative myofibers from triply injured muscles showed that regenerated $Fgf6^{-/-}$ myofibers trended toward reduced size compared with Wt myofibers, barely missing the threshold for statistical significance (Figures 6G and 6H). Taken together, these data suggest that SCs in $Fgf6^{-/-}$ mice retain muscle stem cell function, and that the SC hypoplasia of perinatal origin is stable and preserved through injury-induced regeneration in the adult.

SC increase after perinatal intra-muscular FGF6 protein delivery

The SC hypoplasia of $Fgf6$ mutant mice originates during the second week after birth (Figure 3), as does the SC hyperplasia in mice with myofiber-specific TEAD1 overexpression (Southard et al., 2016). To determine whether FGF6 is sufficient for modulating SC pool size $in\ vivo$, we injected 2 μg of recombinant FGF6 into the right TA of P14 Wt mice, while control siblings received an equal volume of saline. Injected muscles were harvested 6 weeks later at 2 months of age for quantification of SCs (P60; Figure 7A). To detect

SCs, we performed dual anti-PAX7 and anti-Laminin IF on cryosections from saline- and FGF6-injected TA muscles (Figures 7B and 7C). Quantification of sub-laminal PAX7$^+$ cells demonstrated a significant, >50%, increase of SCs in TA muscles in the FGF6 injection group compared with saline-injected controls (Figures 7D and 7E). To determine if myofiber growth was affected by perinatal FGF6 injection, we quantified average muscle fiber sizes, which did not reveal any significant changes (Figure 7F). Additional quantification of myonuclei per myofiber did not reveal any significant differences between perinatal FGF6- and saline-injected TA muscles (Figure 7G). To determine whether the early postnatal period is uniquely plastic to modulating SC number, we probed adult stages by delivering FGF6 to adult (P90) TA muscles (Figure 7H). We performed SC detection 2 weeks post injection via dual anti-PAX7 and anti-Laminin IF (Figures 7I and 7J). By contrast to the increased SCs after perinatal intra-muscular FGF6 injection, adult-specific delivery of FGF6 did not significantly modulate SC numbers (Figure 7K). These data show that FGF6 during the perinatal period is sufficient for SC expansion and further highlight the early postnatal period as a critical window for scaling of the adult SC pool.

A single injury-induced regeneration bout re-scales SCs in perinatally FGF6-injected TA muscles

The SC increase in response to perinatally delivered FGF6 (Figure 7) prompted us to interrogate the regenerative response after acute injury. For this, we injured perinatally FGF6- and control saline-injected TA muscles from 2-month-old mice via intra-muscular cardiotoxin injection and harvested regenerated muscles 2 weeks later (Figure S1A). Histological analysis via H&E staining showed a robust regenerative response in both FGF6- and saline-injected groups indicated by the presence of regenerative myofibers with central nucleation (Figures S1B and S1C). Quantifications of both average myofiber size (Figure S1D) and minimal Feret diameter (Figure S1E), as well as myonuclei number (Figure S1F), did not uncover any significant differences between regenerative myofibers from perinatally FGF6- or saline-injected TA muscles. We then wondered whether the SC increase stemming from a single perinatal FGF6 injection persists in the regenerated TA muscles. We performed SC detection via dual anti-PAX7 and anti-Laminin IF on cryosections from saline- and FGF6-injected regenerative TA muscles (Figures S1G and S1H). Quantification of sub-laminal PAX7$^+$ cells did not reveal any significant differences between SCs of regenerative TA muscles from FGF6- compared with saline-injected samples (Figures S1I and S1J). These data demonstrate that the increased SC pool of perinatally FGF6-injected TA muscles becomes re-scaled similar to control TA muscle SC numbers through a single acute-injury-induced regeneration bout.
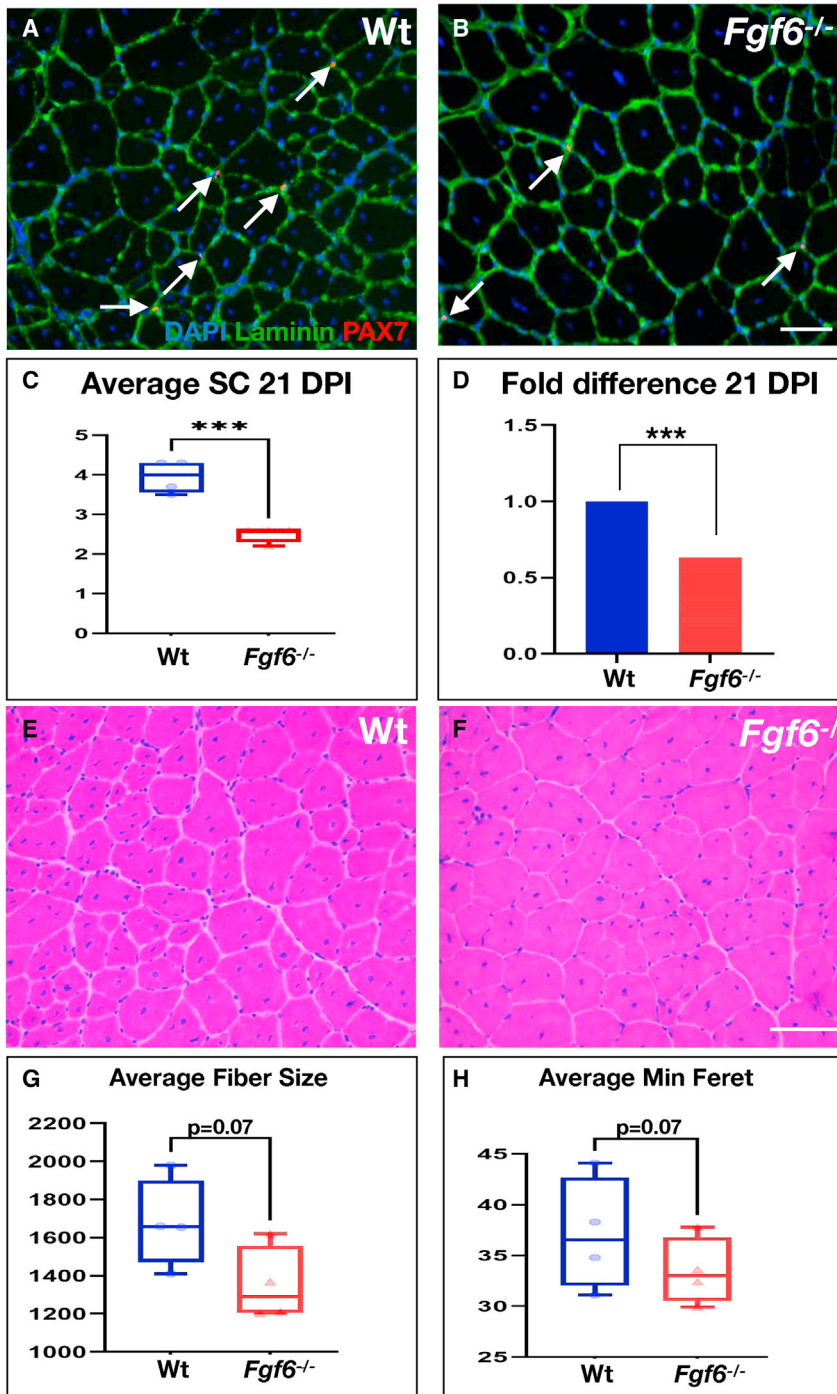
Figure 6. SC hypoplasia persists after injury-induced muscle regeneration

(A and B) Representative dual anti-PAX7/anti-Laminin IF stainings on 10-μm cryosections from 21 DPI TA muscles from Wt (A) and $Fgf6^{-/-}$ (B) mice at 20× magnification; arrows indicate PAX7 (red)-positive nuclei (blue) within the basal lamina (green).

(C and D) Quantification of SCs in regenerated tissue (identified via centrally located myonuclei); average SC numbers per 0.155-mm² area of 10 μm regenerated TA cryosections (C) and normalized as fold difference (D) are displayed; n = 4 adult male mice per genotype; scale bar in (B), 50 μm; paired two-tailed Student's t test: ***p < 0.001.

(E and F) Representative images of H&E-stained 10-μm cryosections of TA muscles from Wt (E) and $Fgf6^{-/-}$ (F) mice at 20× magnification following three consecutive cardiotoxin-induced injury/regeneration cycles, each 21 days apart.

(G and H) Quantification of average triple-regenerated TA muscle fiber size in μm² (G) and minimum Feret in μm (H) from Wt and $Fgf6^{-/-}$ mice; n = 4 four adult male mice for both genotypes tested; scale bar in (F), 50 μm.

DISCUSSION

Here we demonstrate that FGF6 governs muscle stem cell (i.e., SC) pool size *in vivo*. We discover that, in mice lacking *Fgf6*, early postnatal SC proliferation and numbers are reduced, which manifests as SC hypoplasia in the adult.

The mis-regulation of SC number does not affect development and/or growth of myofibers, which are of similar size and number and show a similar myonuclear content to Wt controls. Despite the SC reduction, early regeneration kinetics are not negatively affected; however, later-stage regeneration is compromised, as shown by regenerative
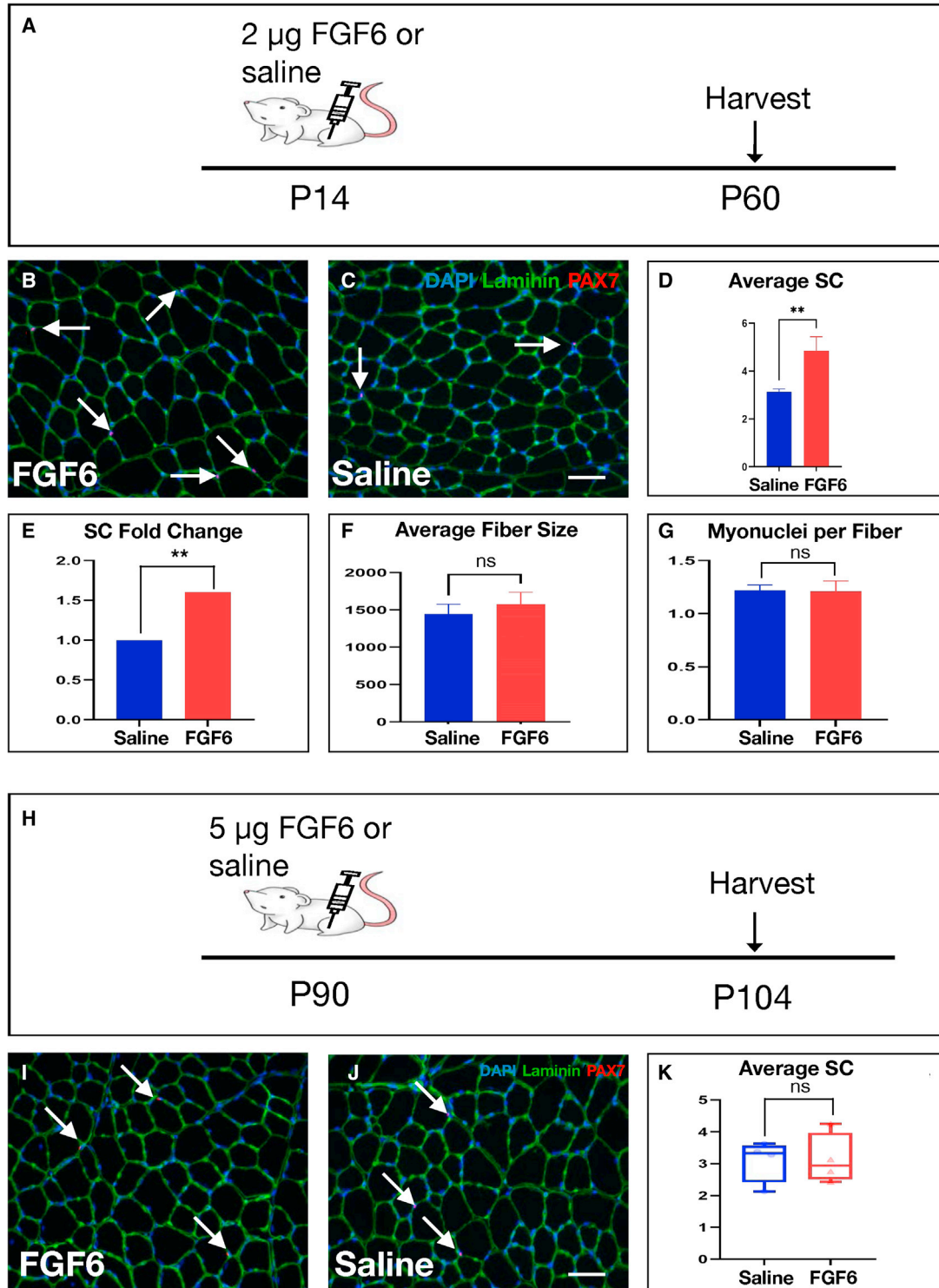
Figure 7. SC increase after perinatal intra-muscular FGF6 protein delivery

(A) Schematic for experimental design: 2 μg of recombinant FGF6 was delivered via injection into the right TA, while the left TA received normal saline as control at P14; TA muscles were harvested at 2 months.

(legend continued on next page)

myofibers of significantly smaller sizes. Interestingly, Schutt et al. (2020) recently reported a similar but mirrored phenomenon. Inactivation of the long non-coding RNA linc-MYH resulted in increased numbers of SCs, which did not enhance skeletal muscle regeneration but increased the cross-sectional area of myofibers, resulting in skeletal muscle hypertrophy. We further show that intra-muscular injection of FGF6 during perinatal stages leads to an expansion of the SC pool, evident at 2 months of age when SCs have entered into quiescence (Gattazzo et al., 2020; White et al., 2010), demonstrating that FGF6 is sufficient to modulate the size of the muscle stem cell pool. Thus, we provide definitive *in vivo* evidence for a role of FGF6 in SC proliferation during a critical postnatal period, contrasting with previous assumptions based on the *in vitro* responsiveness of myoblasts to FGF6 and muscle-specific FGF6 expression (de Lapeyriere et al., 1993; Floss et al., 1997; Han and Martin, 1993; Kastner et al., 2000; Zhao and Hoffman, 2004).

The role of FGF6 in skeletal muscle regeneration

Previous investigations involving acute-injury-induced skeletal muscle regeneration experiments in *Fgf6* mutant mice have led to conflicting conclusions (Fiore et al., 2000; Floss et al., 1997). Floss et al. (1997) reported severe regeneration deficits, including fibrotic scarring, after freeze-crush-induced injury to the TA in *Fgf6* mutant mice. By contrast, Fiore et al. (2000) did not observe any differences in regeneration after snake-venom-induced injury in *Fgf6* mutant mice compared with controls. The re-examination provided here offers insights into the apparent differences. Our injury protocol utilizes snake-venom-induced muscle fiber degeneration similar to the protocol used by Fiore et al. (2000), and we also observed seemingly normal regeneration, as they did. However, Fiore et al. used qualitative assessments of histologically stained sections to conclude a lack of regenerative defects, but our quantification of regenerated muscle fiber size indicates that *Fgf6* is necessary for full regenerative capacity. We propose that the freeze-crush-induced injury used by Floss et al. may indiscriminately cause necrotic cell death, including that of SCs, which would further exacerbate the reduction of the SC pool in *Fgf6* mutant mice (Hardy et al., 2016). Hence, pockets of SC aplasia might arise, resulting in local complete regeneration failure, including fibrotic scarring as reported (Floss et al., 1997).

It is intriguing that, after a regeneration bout, the reduced SC pool size is maintained at defectively scaled pool size in the *Fgf6* mutant. By contrast, the SC hyperplasia resulting from a single intra-muscular FGF6 injection during the early postnatal period is not retained after a single injury-induced regeneration bout. These data suggest contributions from FGF6 to re-scaling the SC pool during regeneration. On the one hand, the return to normal SC numbers in regenerated TA muscles injected with FGF6 during the early postnatal period may reflect that an initially scaled SC pool is not fixed throughout life. On the other hand, SCs are still reduced after regeneration in *Fgf6* mutant mice, which may indicate limited cycling and renewal capacity of the SC pool in the FGF6-deficient regenerative environment. A role for FGF6 in re-scaling the SC pool in skeletal muscle regeneration is further supported by increased FGF6 expression in regenerating muscle tissue (Floss et al., 1997). While the source(s) of this FGF6 expression have yet to be conclusively determined, the finding that isolated myofibers express FGF6 indicates that the nascent regenerative myotubes could be a source (Kastner et al., 2000). Conditional cell-specific *Fgf6* inactivation studies are warranted to unequivocally identify the cellular source of FGF6 expression for SC pool scaling.

The SC reduction in 3-month-old *Fgf6* mutant mice is similar in magnitude to the SC loss in some skeletal muscle groups during aging in both mice and humans (Collins et al., 2007; Fry et al., 2015; Shefer et al., 2006; Verdijk

(B and C) Representative dual anti-PAX7/anti-Laminin IF stainings on 10-μm cryosections from FGF6- (B) and control saline-injected (C) TA muscles at 20× magnification; arrows indicate PAX7 (red)-positive nuclei (blue) within the basal lamina (green); scale bar in (C), 50 μm.

(D and E) Quantification of average SC numbers per 0.155-mm^2 area of 10-μm cryosections (D) and normalized as fold change (E) from saline and FGF6 perinatally injected TA muscles; n = 6 2-month-old mice for each group tested; paired two-tailed Student's t test: **p < 0.01.

(F) Quantification of average muscle fiber size in μm^2 from saline and FGF6 perinatally injected TA muscles; n = 6 2-month-old mice for each group tested; paired two-tailed Student's t test: not significant (ns), p > 0.05.

(G) Myonuclei count normalized to muscle fibers for saline and FGF6 perinatally injected TA muscles; n = 6 2-month-old mice for each genotype; paired two-tailed Student's t test: not significant (ns), p > 0.05.

(H) Schematic for experimental design: 5 μg of recombinant FGF6 was delivered via injection into the right TA, while the left TA received normal saline as control at P90; TA muscles were harvested 2 weeks later (P104).

(I and J) Representative dual anti-PAX7/anti-Laminin IF stainings on 10-μm cryosections from FGF6- (I) and control saline-injected (J) TA muscles at 20× magnification; arrows indicate PAX7 (red)-positive nuclei (blue) within the basal lamina (green); scale bar in (J), 50 μm.

(K) Quantification of average SC numbers per 0.155-mm^2 area of 10-μm cryosections from saline and FGF6-injected TA muscles; n = 5 adult male mice for each group tested; paired two-tailed Student's t test: not significant (ns), p > 0.05. See also Figure S1.

et al., 2014). By contrast, impairment of regenerative capacity is much more pronounced in aged mice compared with young *Fgf6* mutant mice. This suggests that the remaining SCs in *Fgf6* mutant retain muscle stem cell function, while SC-intrinsic and -extrinsic defects accumulating during aging further compromise the functionality of remaining SCs in aged muscle (Hwang and Brack, 2018).

FGF signaling complexity

Our longitudinal quantifications of SC number and proliferation status during the early postnatal period show that SC reductions are evident as early as 2 weeks after birth in *Fgf6* mutant mice. Prior to that, SC numbers and proliferation rates are indistinguishable from Wt mice. However, FGF6 is expressed at much earlier time points during skeletal muscle development in the embryo (Han and Martin, 1993). A likely explanation for the absence of earlier disruptions in myogenesis in *Fgf6* mutant mice is compensatory signaling from other FGFs to stimulate FGFR activation in SCs. Different FGFs can bind to the same FGFRs and stimulate mitogenic activity of the cell (Zhang et al., 2006). Other FGFs expressed in the skeletal muscle lineage (including FGF1, FGF2, FGF4, FGF5, and FGF7; Hannon et al., 1996; Kastner et al., 2000) may mask the lack of FGF6 early in development. As postnatal muscle development progresses, the total pool of FGF ligands available to regulate SCs via binding to FGFR1 and FGFR4 may become more limiting and, hence, result in reduced mitogenic stimulation of SCs in mice lacking FGF6. Alternatively, other growth factors, e.g., HGF or IGF-1, may dominate in embryonic and early postnatal development, thereby masking the role of FGF signaling. Additional studies probing for contributions from other FGFs and the combined contributions of both FGFR1 and FGFR4 to SC pool sizing, as well as other growth factors and their receptors, are needed.

Dynamic SC regulation during early postnatal stages

Developmental myofiber growth and entry of SCs into quiescence to establish the adult muscle stem cell pool are intricately linked. Lineage tracing of PAX7+ SCs during the first 3 weeks after birth in the mouse revealed a gradual decline in fusion of SCs with existing myofibers (Lepper et al., 2009). Longitudinal quantification of myonuclei further revealed that myofibers complete acquisition of adult nuclei numbers by 3 weeks after birth (White et al., 2010). By extension, these data imply that the SC fraction escaping differentiation and fusion with myofibers is available for generating the quiescent muscle stem cell pool for muscle fiber repair and regeneration, or hypertrophy in the adult. In this model, the muscle fiber determines the number of SC fusion events for myonuclei increase and fiber growth. This can explain why *Fgf6*

mutant mice do not show reduced myofiber size or myonuclei number despite reduced SC proliferation at 2 weeks after birth. Instead, the reduced SC proliferation only compromises the pool of SCs available in adulthood, resulting in SC hypoplasia. Our previous analysis of the TEAD1-Tg mouse model conversely featured increased perinatal SC proliferation and SC hyperplasia in adulthood (Southard et al., 2016). The increase in SCs in that model was not accompanied by any myofiber hyperplasia or hypertrophy, which may further support a model in which the myofiber dictates total SC fusion, independent of the number of available SCs. Taken together, early postnatal myofiber growth appears to be relatively inert to alterations in perinatal SC availability. While the tolerable threshold in which the SC pool size does not affect myofiber growth has not yet been defined precisely, we reason, based on the *Fgf6* mutant and TEAD-1 Tg models, that skeletal muscles are able to deal with a rather large range. This concept has important implications for the design of biomedical strategies for increasing myofiber size and/or strength via expansion of the pool of SCs.

EXPERIMENTAL PROCEDURES

Animals

Fgf6−/− mutant mice were previously described (Floss et al., 1997). The *Fgf6* loss-of-function allele was maintained on a mixed C57BL/6 and 129sv genetic background. *Fgf6*−/− mutant and age-matched Wt sibling mice were obtained from *Fgf6*+/− heterozygous intercrosses. Acute muscle injury experiments were performed by injecting 30 μL of cardiotoxin (5 μM in pharmaceutical grade normal saline; Sigma C9759) into the right TA of adult mice after anesthesia by intra-peritoneal delivery of ketamine/xylazine (87.5/12 mg/kg respectively; in pharmaceutical grade normal saline). For repeated injury experiments, TA muscles were injected with 30 μL of cardiotoxin (5 μM) for each injury and allowed to regenerate for 21 days between injuries. EdU (Thermo Fisher A10044) was administered via a single subcutaneous injection to mouse pups (5 mg/kg; in pharmaceutical grade normal saline). Recombinant human FGF-6 protein (Novus Biologicals NBP2-76275) was delivered via 5-μL intra-muscular injection into the TA by Hamilton syringe after anesthesia by isoflurane (induction with 5% and maintenance with 2%; Henry Schein NDC11695-6776-2). All animals and procedures were approved by IACUC protocol # 2018A00000136.

PCR genotyping

Tissue collection for genotyping by PCR was done by ear punch. Genomic DNA was extracted using the ExtractN'Amp kit (Sigma XNAT2) following the manufacturer's instructions. PCR reactions were done using GoTaq polymerase (Promega M8291) following manufacturer's instructions. Primer sequences were as follows: *Fgf6 ex1b*, 5′CTGCAGGCTTCGTCTTCTT; *Fgf6 ex1c*, 5′AGAGTCTC CGCTGTCGCTTA; *neo*, 5′GCCAGAGGCCACTTGTGTAGCG. PCR products were resolved in a 2% agarose gel, stained with 0.5 μg/mL

ethidium bromide (Gibco 15585011), and digitally imaged with a Bio-Rad Gel Doc system for record keeping.

IF

For IF staining, muscles were isolated and flash frozen in isopentane chilled in liquid nitrogen. Samples were cryo-sectioned at 10 μm and collected on Histobond slides (Azer Scientific UNI75251+). Tissue sections were fixed for 10 min in 4% paraformaldehyde/phosphate-buffered saline (PBS), washed twice with PBS, and permeabilized with 0.3% Triton-X/PBS for 20 min. After a rinse with PBT (0.05% Triton-X/PBS), samples were incubated with M.O.M. blocking reagent (Vector Laboratories BMK-2202) in a humidified chamber for up to 3 h. Next, the sections were blocked with goat blocking solution (1% Blocking Powder [Perkin Elmer, FP1012]/10% goat serum in PBT) for 30 min, and then incubated with primary antibodies (diluted in goat blocking solution) in the humidified chamber overnight at 4°C. Antibodies and dilutions used were as follows: anti-PAX7 (1:5; PAX7 was deposited to the Developmental Studies Hybridoma Bank by Kawakami, A.; RRID: AB_528428); anti-Laminin (1:1,000; Sigma L9393; RRID: AB_477163); and anti-dystrophin (1:100; MANDRA1(7A10) was deposited to the DSHB by Morris, G.E.; RRID: AB_2618143). The following day, after three 10-min washes with PBT, sections were incubated with appropriate secondary antibodies diluted 1:1,000 in goat blocking solution for 1 h at room temperature. Secondary antibodies used were as follows: goat anti-rabbit IgG Alexa488 (Invitrogen A11034; RRID: AB_2576217) and anti-mouse IgG1 Alexa568 (Invitrogen A-21124; RRID: AB_2535766). Samples were counterstained with DAPI and washed three times with PBT. Slides were mounted with Fluoromount (SouthernBiotech 0100-01) and an appropriately sized coverslip, with nail polish being used to fixate cover slips and prevent drying out of samples. All IF images were obtained using a Zeiss Axioscope microscope and a Zeiss AxioCam monochrome charge-coupled device (CCD) camera.

EdU proliferation assays

Two hours prior to harvesting of hindlimb muscles, EdU was administered to pups via subcutaneous injection at a dosage of 5 mg/kg bodyweight. EdU detection followed incubation with secondary antibodies using the Click-iT Kit (Invitrogen C10640) and following the manufacturer's instructions.

Histology

For H&E stainings, cryopreserved muscles were sectioned at 10-μm thickness and collected on Histobond slides (Azer Scientific UNI75251+). Samples were then fixed at room temperature in 100% ethanol for 30 s, followed by a 1-min wash in tap water. The samples were then stained with Gill's II hematoxylin for 4.5 min, washed with running lukewarm tap water, treated with Scott's tap water for 10 s, and washed again in tap water for an additional 1 min. Eosin was used to stain the samples for 45 s, followed by destaining in ethanol (four dips in 70% ethanol, seven dips in 90% ethanol, 10 dips in 100% ethanol) and Histoclear 1 (10 dips) and Histoclear 2 (10 dips). Mounting was performed with Cytoseal-60 and an appropriately sized coverslip. All images were obtained via bright-field microscopy using a ToupCam camera (UCMOS05100KPA).

Quantifications (fiber size, SCs, fiber number, myonuclei)

All quantifications were performed blinded to the samples' genotypes.

Muscle size was determined by anti-Laminin IF stainings of 10-μm muscle cross sections counterstained with DAPI. Average fiber size and minimum Feret were quantified via creating Laminin and DAPI overlays in ImageJ software, and processing and quantifying the overlays in SMASH (Smith and Barton, 2014). IF stains were also used to quantify average regenerative muscle size and minimum Feret. For 3.5- and 5-DPI muscle samples, fibers were manually outlined and measured via ImageJ since regenerative fiber sizes were too small for detection by SMASH.

SC detection was performed via IF stainings of 10-μm cross sections using anti-PAX7 and anti-Laminin, and counterstaining with DAPI. Images were taken randomly by imaging the anti-Laminin signal first, followed by anti-PAX7 to avoid any potential bias in selecting areas for imaging. Images for each channel were taken at 20× magnification, overlaid using ImageJ software, and sublaminal PAX7$^+$ SCs were manually counted.

For EDL fiber quantification, images of H&E-stained EDL cross sections at 4× magnification were counted manually. IF stains were used for myonuclei quantification in 10-μm cross sections using anti-dystrophin and DAPI counterstaining. Images were taken at 20× magnification, overlaid in ImageJ, and nuclei number normalized to total fiber number were determined manually by counting myonuclei (DAPI$^+$ within the dystrophin$^+$ domains) and myofibers.

Statistics

GraphPad Prism 9 was used for box and whisker plots, and bar graphs to visualize data. Error bars in histograms represent standard deviation (SD) over the mean. All data were subjected to a two-tailed t test to determine statistically significant differences. Statistical significance was determined as a p value <0.05. Sample sizes were predetermined based on published SC counts, which reveal very low variability, and on preliminary data revealing a highly robust and reproducible SC reduction in TA muscles of both male and female *Fgf6* mutant mice.

Data and code availability

All data are contained within the article.

AUTHOR CONTRIBUTIONS

W.Z. performed all experiments, quantifications, data analysis, and figure assembly and contributed to writing the manuscript. S.S. performed preliminary characterization of *Fgf6* mutant mice. T.B. contributed the *Fgf6* mutant mouse strain and edited the manuscript. C.L. conceived the study, designed experiments, blinded

REFERENCES

Allbrook, D.B., Han, M.F., and Hellmuth, A.E. (1971). Population of muscle satellite cells in relation to age and mitotic activity. Pathology *3*, 223–243.

Boldrin, L., and Morgan, J.E. (2012). Human satellite cells: identification on human muscle fibres. PLoS Curr. *3*, RRN1294.

Collins, C.A., Olsen, I., Zammit, P.S., Heslop, L., Petrie, A., Partridge, T.A., and Morgan, J.E. (2005). Stem cell function, self-renewal, and behavioral heterogeneity of cells from the adult muscle satellite cell niche. Cell *122*, 289–301.

Collins, C.A., Zammit, P.S., Ruiz, A.P., Morgan, J.E., and Partridge, T.A. (2007). A population of myogenic stem cells that survives skeletal muscle aging. Stem Cells *25*, 885–894.

Cornelison, D.D., Filla, M.S., Stanley, H.M., Rapraeger, A.C., and Olwin, B.B. (2001). Syndecan-3 and syndecan-4 specifically mark skeletal muscle satellite cells and are implicated in satellite cell maintenance and muscle regeneration. Dev. Biol. *239*, 79–94.

de Lapeyriere, O., Ollendorff, V., Planche, J., Ott, M.O., Pizette, S., Coulier, F., and Birnbaum, D. (1993). Expression of the Fgf6 gene is restricted to developing skeletal muscle in the mouse embryo. Development *118*, 601–611.

Fiore, F., Sebille, A., and Birnbaum, D. (2000). Skeletal muscle regeneration is not impaired in Fgf6$^{-/-}$ mutant mice. Biochem. Biophys. Res. Commun. *272*, 138–143.

Flanagan-Steet, H., Hannon, K., McAvoy, M.J., Hullinger, R., and Olwin, B.B. (2000). Loss of FGF receptor 1 signaling reduces skeletal muscle mass and disrupts myofiber organization in the developing limb. Dev. Biol. *218*, 21–37.

Floss, T., Arnold, H.H., and Braun, T. (1997). A role for FGF-6 in skeletal muscle regeneration. Genes Dev. *11*, 2040–2051.

Fry, C.S., Lee, J.D., Mula, J., Kirby, T.J., Jackson, J.R., Liu, F., Yang, L., Mendias, C.L., Dupont-Versteegden, E.E., McCarthy, J.J., et al. (2015). Inducible depletion of satellite cells in adult, sedentary mice impairs muscle regenerative capacity without affecting sarcopenia. Nat. Med. *21*, 76–80.

Gattazzo, F., Laurent, B., Relaix, F., Rouard, H., and Didier, N. (2020). Distinct phases of postnatal skeletal muscle growth govern the progressive establishment of muscle stem cell quiescence. Stem Cell Reports *15*, 597–611.

Gros, J., Manceau, M., Thome, V., and Marcelle, C. (2005). A common somitic origin for embryonic muscle progenitors and satellite cells. Nature *435*, 954–958.

Grounds, M.D., and McGeachie, J.K. (1989). A comparison of muscle precursor replication in crush-injured skeletal muscle of Swiss and BALBc mice. Cell Tissue Res. *255*, 385–391.

Han, J.K., and Martin, G.R. (1993). Embryonic expression of Fgf-6 is restricted to the skeletal muscle lineage. Dev. Biol. *158*, 549–554.

Hannon, K., Kudla, A.J., McAvoy, M.J., Clase, K.L., and Olwin, B.B. (1996). Differentially expressed fibroblast growth factors regulate skeletal muscle development through autocrine and paracrine mechanisms. J. Cell Biol. *132*, 1151–1159.

Hardy, D., Besnard, A., Latil, M., Jouvion, G., Briand, D., Thepenier, C., Pascal, Q., Guguin, A., Gayraud-Morel, B., Cavaillon, J.M., et al. (2016). Comparative study of injury models for studying muscle regeneration in mice. PLoS One *11*, e0147198.

Hellmuth, A.E., and Allbrook, D.B. (1971). Muscle satellite cell numbers during the postnatal period. J. Anat. *110*, 503.

Hwang, A.B., and Brack, A.S. (2018). Muscle stem cells and aging. Curr. Top. Dev. Biol. *126*, 299–322.

Kastner, S., Elias, M.C., Rivera, A.J., and Yablonka-Reuveni, Z. (2000). Gene expression patterns of the fibroblast growth factors and their receptors during myogenesis of rat satellite cells. J. Histochem. Cytochem. *48*, 1079–1096.

Lepper, C., Conway, S.J., and Fan, C.M. (2009). Adult satellite cells and embryonic muscle progenitors have distinct genetic requirements. Nature *460*, 627–631.

Lepper, C., and Fan, C.M. (2010). Inducible lineage tracing of Pax7-descendant cells reveals embryonic origin of adult satellite cells. Genesis *48*, 424–436.

Lepper, C., Partridge, T.A., and Fan, C.M. (2011). An absolute requirement for Pax7-positive satellite cells in acute injury-induced skeletal muscle regeneration. Development *138*, 3639–3646.

Luz, M.A., Marques, M.J., and Santo Neto, H. (2002). Impaired regeneration of dystrophin-deficient muscle fibers is caused by exhaustion of myogenic cells. Braz. J. Med. Biol. Res. *35*, 691–695.

Mauro, A. (1961). Satellite cell of skeletal muscle fibers. J. Biophys. Biochem. Cytol. *9*, 493–495.

McCarthy, J.J., Mula, J., Miyazaki, M., Erfani, R., Garrison, K., Farooqui, A.B., Srikuea, R., Lawson, B.A., Grimes, B., Keller, C., et al. (2011). Effective fiber hypertrophy in satellite cell-depleted skeletal muscle. Development *138*, 3657–3666.

Moss, F.P., and Leblond, C.P. (1970). Nature of dividing nuclei in skeletal muscle of growing rats. J. Cell Biol. *44*, 459–462.

Murphy, M.M., Lawson, J.A., Mathew, S.J., Hutcheson, D.A., and Kardon, G. (2011). Satellite cells, connective tissue fibroblasts and their interactions are crucial for muscle regeneration. Development *138*, 3625–3637.

Ontell, M., Feng, K.C., Klueber, K., Dunn, R.F., and Taylor, F. (1984). Myosatellite cells, growth, and regeneration in murine dystrophic muscle: a quantitative study. Anat. Rec. *208*, 159–174.

Ontell, M., and Kozeka, K. (1984). The organogenesis of murine striated muscle: a cytoarchitectural study. Am. J. Anat. *171*, 133–148.

Ornitz, D.M., and Itoh, N. (2001). Fibroblast growth factors. Genome Biol. *2*, REVIEWS3005.

Oustanina, S., Hause, G., and Braun, T. (2004). Pax7 directs postnatal renewal and propagation of myogenic satellite cells but not their specification. EMBO J. *23*, 3430–3439.

Pawlikowski, B., Vogler, T.O., Gadek, K., and Olwin, B.B. (2017). Regulation of skeletal muscle stem cells by fibroblast growth factors. Dev. Dyn. *246*, 359–367.

Relaix, F., Montarras, D., Zaffran, S., Gayraud-Morel, B., Rocancourt, D., Tajbakhsh, S., Mansouri, A., Cumano, A., and Buckingham, M. (2006). Pax3 and Pax7 have distinct and overlapping functions in adult muscle progenitor cells. J. Cell Biol. *172*, 91–102.

Relaix, F., Rocancourt, D., Mansouri, A., and Buckingham, M. (2005). A Pax3/Pax7-dependent population of skeletal muscle progenitor cells. Nature *435*, 948–953.

Reznik, M. (1969). Thymidine-3H uptake by satellite cells of regenerating skeletal muscle. J. Cell Biol. *40*, 568–571.

Rosen, G.D., Sanes, J.R., LaChance, R., Cunningham, J.M., Roman, J., and Dean, D.C. (1992). Roles for the integrin VLA-4 and its counter receptor VCAM-1 in myogenesis. Cell *69*, 1107–1119.

Sacco, A., Doyonnas, R., Kraft, P., Vitorovic, S., and Blau, H.M. (2008). Self-renewal and expansion of single transplanted muscle stem cells. Nature *456*, 502–506.

Sambasivan, R., Yao, R., Kissenpfennig, A., Van Wittenberghe, L., Paldi, A., Gayraud-Morel, B., Guenou, H., Malissen, B., Tajbakhsh, S., and Galy, A. (2011). Pax7-expressing satellite cells are indispensable for adult skeletal muscle regeneration. Development *138*, 3647–3656.

Schienda, J., Engleka, K.A., Jun, S., Hansen, M.S., Epstein, J.A., Tabin, C.J., Kunkel, L.M., and Kardon, G. (2006). Somitic origin of limb muscle satellite and side population cells. Proc. Natl. Acad. Sci. U S A *103*, 945–950.

Schultz, E. (1974). A quantitative study of the satellite cell population in postnatal mouse lumbrical muscle. Anat. Rec. *180*, 589–595.

Schultz, E., Gibson, M.C., and Champion, T. (1978). Satellite cells are mitotically quiescent in mature mouse muscle: an EM and radioautographic study. J. Exp. Zool. *206*, 451–456.

Schutt, C., Hallmann, A., Hachim, S., Klockner, I., Valussi, M., Atzberger, A., Graumann, J., Braun, T., and Boettger, T. (2020). Linc-MYH configures INO80 to regulate muscle stem cell numbers and skeletal muscle hypertrophy. EMBO J. *39*, e105098.

Seale, P., Sabourin, L.A., Girgis-Gabardo, A., Mansouri, A., Gruss, P., and Rudnicki, M.A. (2000). Pax7 is required for the specification of myogenic satellite cells. Cell *102*, 777–786.

Sheehan, S.M., and Allen, R.E. (1999). Skeletal muscle satellite cell proliferation in response to members of the fibroblast growth factor family and hepatocyte growth factor. J. Cell Physiol. *181*, 499–506.

Shefer, G., Van de Mark, D.P., Richardson, J.B., and Yablonka-Reuveni, Z. (2006). Satellite-cell pool size does matter: defining the myogenic potency of aging skeletal muscle. Dev. Biol. *294*, 50–66.

Smith, L.R., and Barton, E.R. (2014). SMASH - semi-automatic muscle analysis using segmentation of histology: a MATLAB application. Skelet Muscle *4*, 21.

Snow, M.H. (1977). Myogenic cell formation in regenerating rat skeletal muscle injured by mincing. II. An autoradiographic study. Anat. Rec. *188*, 201–217.

Southard, S., Kim, J.R., Low, S., Tsika, R.W., and Lepper, C. (2016). Myofiber-specific TEAD1 overexpression drives satellite cell hyperplasia and counters pathological effects of dystrophin deficiency. eLife *5*, e15461.

Verdijk, L.B., Snijders, T., Drost, M., Delhaas, T., Kadi, F., and van Loon, L.J. (2014). Satellite cells in human skeletal muscle; from birth to old age. Age (Dordr) *36*, 545–547.

White, R.B., Bierinx, A.S., Gnocchi, V.F., and Zammit, P.S. (2010). Dynamics of muscle fibre growth during postnatal mouse development. BMC Dev. Biol. *10*, 21.

Yablonka-Reuveni, Z., Danoviz, M.E., Phelps, M., and Stuelsatz, P. (2015). Myogenic-specific ablation of Fgfr1 impairs FGF2-mediated proliferation of satellite cells at the myofiber niche but does not abolish the capacity for muscle regeneration. Front. Aging Neurosci. *7*, 85.

Zhang, X., Ibrahimi, O.A., Olsen, S.K., Umemori, H., Mohammadi, M., and Ornitz, D.M. (2006). Receptor specificity of the fibroblast growth factor family. The complete mammalian FGF family. J. Biol. Chem. *281*, 15694–15700.

Zhao, P., and Hoffman, E.P. (2004). Embryonic myogenesis pathways in muscle regeneration. Dev. Dyn. *229*, 380–392.